Pergamon

Journal of Structural Geology, Vol. 17, No. 9, pp. 1217 to 1231, 1995

0191-8141/95 $9.50+0.00

0191-8141(95)00025-9

Strain and possible volume loss in a high-grade ductile shear zone

HARI B. SRIVASTAVA*, PETER HUDLESTON and DRUMMOND EARLEY III†

Department of Geology and Geophysics, University of Minnesota, Minneapolis, MN 55455, U.S.A.

(*Received* 26 *April* 1994; *accepted in revised form* 4 *February* 1995)

Abstract—Small-scale ductile shear zones in high-grade metagabbros from the Caledonides of northern Sweden provide a good opportunity for examining the development of fabric and strain in rocks undergoing progressive non-coaxial deformation. The rocks contain strain markers in the form of aggregates of plagioclase feldspar. A selected shear zone is analyzed assuming monoclinic symmetry, which requires for the zone as a whole variable simple shear, variable volume change, or variable simple shear and volume change plus a homogeneous deformation. Both size of the feldspar aggregates and aspect ratio of the aggregates plotted against orientation indicate significant volume decrease (in excess of 50%, and perhaps as much as 80%) towards the centers of the zones. The data are broadly consistent with a deformation path involving constant shear strain across the zone followed by variable volume change *or* by a path of progressive loss of volume with increasing shear strain followed by a homogeneous strain. They are *not* consistent with a single path involving rates of shear strain and volume loss that are in constant proportions.

There is little difference in chemical composition between the shear zone and the surrounding rock. An analysis of the concentrations of elements in the shear zone and wall rock suggests that volume changes were slight ($< \pm 15\%$). The discrepancy between the values of volume change estimated from strain analysis and geochemical analysis may be resolved either by geochemical equilibration being attained after deformation or by a departure from the geometric constraints of the monoclinic 'band' model for shear zones. Modification of marker particle size and shape during dynamic recrystallization may also partly account for the apparent volume loss.

INTRODUCTION

DUCTILE shear zones are common features in crystalline rocks that have undergone natural deformation at moderate to high temperatures (e.g. Choukroune & Gapais 1983, Ramsay & Allison 1979). They vary in width from millimeters to kilometers and displacements along them may vary from the same order of dimension as the width to several orders of magnitude larger (e.g. Ramsay & Graham 1970, Hara *et al.* 1973, Coward 1974, Mitra 1975, Bell 1981, Carter 1992, Mohanty & Ramsay 1994). They typically display, when viewed in a section perpendicular to the plane of shear and parallel to the shear direction, a foliation with sigmoidal trace across the zone, increasing in intensity from the edges towards the center. A lineation is usually developed in the foliation, with a projection on the shear plane in the shear direction (Lin & Williams 1992). The increase in foliation intensity can be related to an increase in strain intensity and commonly also to a better developed crystallographic fabric (e.g. Ramsay & Graham 1970, Hudleston 1977, Simpson 1983, Lloyd *et al.* 1992). The foliation within a shear zone may develop in a heterogeneous way, giving rise to *S*–*C* structures (e.g. Berthé *et al.* 1979), and it may be affected by subsequent folding, boudinage or shear band development (e.g. Platt & Vissers 1980, Lister & Snoke 1984, Hanmer 1986).

Ramsay & Graham (1970) have shown that for a parallel-sided shear zone with monoclinic symmetry in which there is no gradient in fabric or strain parallel to the zone in the symmetry plane, and for which there is no deformation outside the zone, the deformation within the zone can *only* be one of variable simple shear, variable volume change or a combination of the two (although deviations from this are possible if strain partitioning on a finer scale occurs within the shear zone—see for example fig. 14 of Lister & Williams 1979). The coordinate system used to describe this geometry is shown in Fig. 1. The shear plane is the *xy*-plane and *x* is the shear direction. This basic geometry also allows for the presence of a homogeneous strain, affecting shear zone and wall rock alike (see also Cobbold 1977, and Schwerdtner 1982). Ductile shear zones which possess these geometric properties provide excellent opportunities to study the progressive development of textural and structural changes with changes in state of strain in a non-coaxial regime (e.g. Hudleston 1977, Lister & Williams 1979, Lloyd *et al.* 1992, Mohanty &

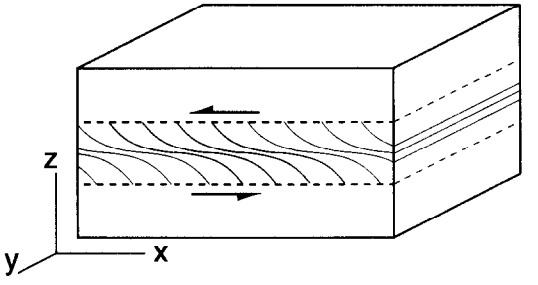

Fig. 1. Coordinate system used to describe the geometry of the shear zones.

*Present address: Department of Geology, Banaras Hindu University, Varanasi, 221005, India.

†Present address: U.S. Bureau of Mines, Twin Cities Research Center, 5629 Minnehaha Ave. S., Minneapolis, MN 554, U.S.A.

Ramsay 1994). In practice, of course, all shear zones deviate from the ideal geometric configuration, typically in that the walls of the zones are neither exactly straight or parallel, and in that shear zones have terminations (Coward 1976, Ramsay 1980, fig. 17). Also, shear zones are often found in an anastomosing pattern, with the same or opposite senses of displacement on coalescing zones (Ramsay & Allison 1979, Choukroune & Gapais 1983, Simpson, 1983, Gapais *et al.* 1987).

In many analyses of strain and fabric in shear zones, it is assumed that deformation occurs without change in volume (e.g. Coward 1976, Kerrich *et al.* 1977, Burg & Laurent 1978, Naruk 1986). This is a difficult assumption to test, and in most cases there is insufficient information to determine volume change independently. Since fluids are involved in deformation under a wide range of metamorphic conditions and are mobile in much of the crust (e.g. Etheridge *et al.* 1984, Andersen *et al.* 1991, Schedl *et al.* 1992), it seems likely that material will be removed or introduced during deformation. Supportive of this is the observation that mineralogical and chemical changes are commonly found in association with ductile shear zones (e.g. Beach 1976, Mitra 1978, Gilotti 1989, Dipple *et al.* 1990, Gates & Speer 1991). In fact, where it is possible to estimate volume change, volume losses have usually been recorded (e.g. Schwerdtner 1982, Mawer 1983, O'Hara 1988, 1990, Glazner & Bartley 1991, Newman & Mitra 1993).

In the present work, we examine several small shear zones developed under upper amphibolite/granulite facies conditions of metamorphism in amphibolites/metagabbros from the northern Swedish Caledonides. These rocks present advantages for analysis because they possess well-defined aggregates of recrystallized feldspar, which make good strain markers. *Shape* and *orientation* of the feldspar aggregates provide a means of determining both strain and volume change within the shear zones. The *size* of the aggregates provides an independent means of determining volume change. If we make the normal assumptions about the geometry of shear zones—that is that they are monoclinic planar bands—we are led to infer that volume loss has occurred in conjunction with shear strain in these rocks. An additional estimate of volume change within the shear zones is provided by geochemical analysis, and a discrepancy between this estimate and the other estimates of volume change leads us to question the reliability of the strain markers, the 'band model' of shear zones used in the geometric analysis and the significance of the isochemical state of the shear zone and its wall rock.

GEOLOGICAL SETTING

The shear zones are developed in rocks of the Caledonide Seve-Köli nappe complex in northern Sweden (Swedish Lapland) (Fig. 2). These and underlying nappes have been thrust from the west to overlie thin Cambrian strata and the basement rocks of the Baltic Shield (Gee & Zachrisson 1979). The host rocks are metagabbros that form part of the Eastern Amphibolites (Kulling 1964, Strand & Kulling 1972), and the best samples of shear zones were found in boulders in valleys just to the east of the mountain of Kebnekaise. The samples are thus not oriented, and the relationship of the fabric in the amphibolites to the thrusting event is not known.

The rock is composed principally of hornblende, quartz, garnet, plagioclase feldspar and clinopyroxene (diopside). Textures in the rock are consistent with an equilibrium metamorphic mineral assemblage, with polygonal grains and sharp, well-defined grain boundaries for all phases. Similar textures inside and outside the shear zones indicate that deformation was synchronous with metamorphism or that peak metamorphism outlasted deformation. The textural evidence for equilibrium conditions and the existence of suitable assemblages of phases allow pressure and temperature estimates of conditions during metamorphism and deformation to be made (for details see the Appendix). The temperatures of about 800°C and pressures of 9–14 kb so obtained indicate upper amphibolite to granulite facies conditions. Thus the deformation that produced the shear zones occurred near the base of the crust (if of normal thickness) and either preceded nappe emplacement or represented its earliest expression.

Most of the description that follows refers to one sample selected for detailed analysis. Measurements of feldspar aggregate shapes were also made on field photographs of shear zones. The results are similar to those presented here.

GEOMETRY AND TEXTURE OF SHEAR ZONES

The rock, both outside and within the shear zones, consists predominantly of plagioclase and hornblende. The white patches prominent on cut and polished surfaces or in outcrop (Figs. 3a–c) are recrystallized aggregates of plagioclase, presumably once feldspar phenocrysts or porphyroblasts. These are drawn out into a foliation within the shear zones, and this foliation displays the sigmoidal pattern characteristic of ductile shear zones (Figs. 3a & b). It becomes progressively better developed towards the center of the zones, where the aspect ratio of the aggregates is highest and where the inclination of the long axes of the aggregates to the boundary of the shear zone is smallest. In any one zone, the sense of shear is consistent. In the centers of some of the shear zones, the feldspar aggregates can no longer be distinguished—they become nebulous and seemingly absorbed into the matrix.

The full dimensions of the shear zones could not be assessed, but those studied are up to a few centimeters wide and have aspect ratios in the displacement direction of at least 10:1 (Fig. 3a). For a selected shear zone, isogons (Fig. 5) are drawn on a section perpendicular to the plane of shear and also perpendicular to the axis of the fold formed by the foliation as it curves into the shear zone. These show a modest degree of parallelism in the

central part of the shear zone and thus indicate a rough approximation to the ideal monoclinic symmetry required for the shear band model. The angle between the foliation and the shear zone boundaries varies from about 40° away from the zone to almost 0° at the center. In another section perpendicular to the first and parallel to the fold axis for the curved foliation, the feldspar aggregates are elongate parallel to the shear zone both within and outside the zone (Fig. 3c), indicating a component of bulk deviatoric stretch affecting the whole rock. As in the first section and as expected, the aspect ratios of the aggregates are higher in the shear zone than outside.

The minerals of all species occur as fairly equiaxed polygonal grains that are much smaller than the feldspar aggregates (which are up to about 4 mm in diameter in the undeformed rock). Grain size is fairly uniform, and typically about 0.02 mm. In thin section, a weak banding is apparent within the shear zones, with some bands showing slight grain refinement and others moderate grain enlargement (Fig. 4a). Grain size in the coarsest band is about 0.04 mm. The feldspar aggregates are made up almost entirely of plagioclase (with some clinozoisite), which is similar in grain size to the surrounding rock. Closer inspection shows that the grains are not, in fact, truly equiaxed, and that there is a weakly-developed grain-shape fabric with a preferred alignment of grains oblique to the plane of shear. This is demonstrated by using the SURFOR wheel method of Panozzo (1987). The numbers of intersections of grain boundaries encountered in linear traverses in different directions were counted on a photograph of a thin section, and the numbers of intersections are plotted against orientation of the line. On the plot the minimum and maximum number of intersections represent the orientations of maximum and minimum grain dimensions respectively and their ratio is the mean grain-shape fabric ellipse (inset in Fig. 4b). This would be the 'strain ratio' for initially equiaxed grains. Grain-shape fabric ellipses with axial ratios of about 1.4 to 1.5 were found,

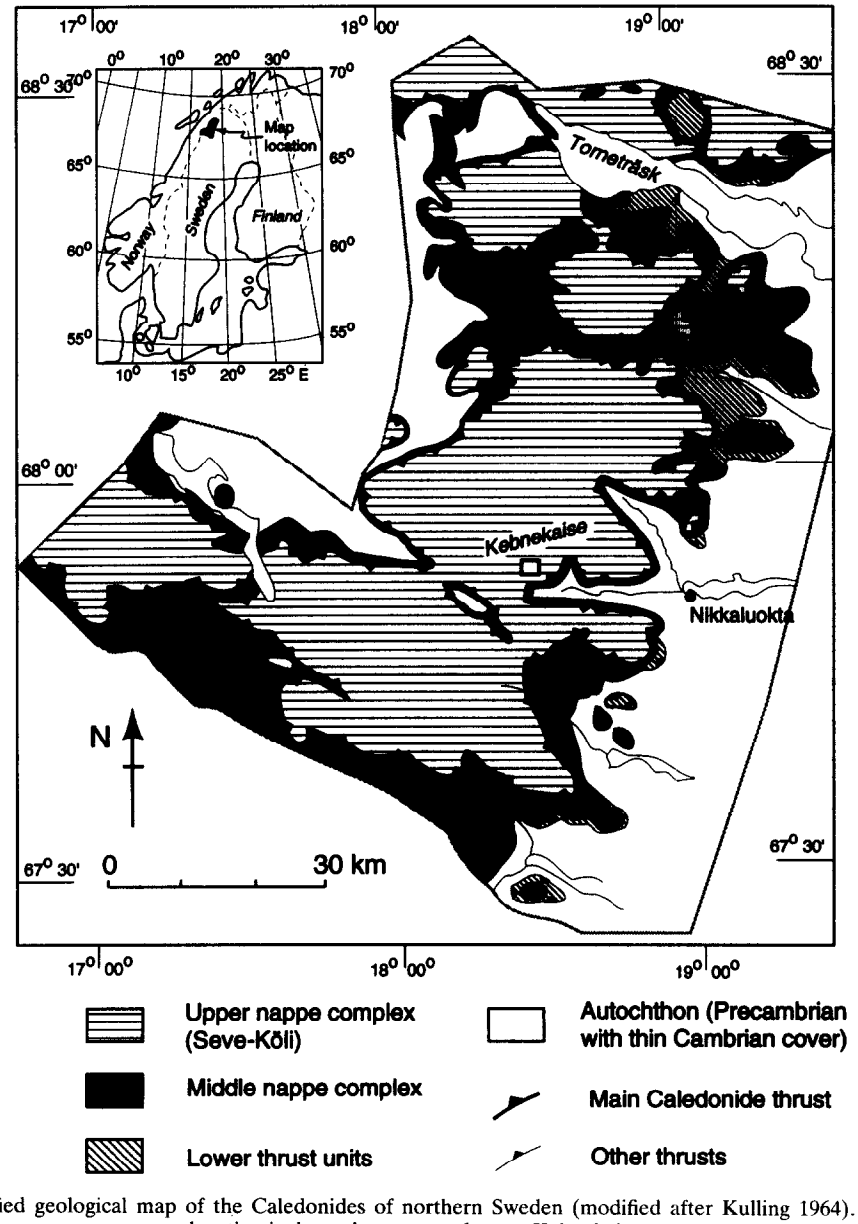

Fig. 2. Simplified geological map of the Caledonides of northern Sweden (modified after Kulling 1964). The sample location is shown by a rectangle near Kebnekaise.

with the long axes at about 40–45° to the shear zone boundaries. The sense of obliquity of this ellipse is consistent with the sense of shear known for the shear zone from the feldspar aggregates. This is a weak example of a recrystallized grain-shape fabric that is often pronounced in quartz mylonites (Lister & Snoke 1984). To achieve the observed textures and large strains, deformation mechanisms of diffusional creep, intracrystalline plasticity, and grain-boundary sliding would have been active in some combination, with a high degree of grain-boundary mobility. We have not measured the crystallographic quartz fabric in the rock but, under crossed nicols in thin section, there is little visible evidence for a preferred crystallographic orientation.

STRAIN ANALYSIS

Strain within shear zones can be computed using deformed objects, rotated veins and dikes that transect the shear zone, or the attitude of foliation in the zone (Ramsay & Graham 1970). For all but deformed objects, the plane of shear must be known and used as a reference orientation for measuring angles. In the shear zones under investigation, aggregates of feldspar are present throughout the rock and provide excellent strain markers. In addition, the plane of shear (as represented by the mean orientation of the isogons) is reasonably well defined. We assume in this analysis that the feldspar aggregates behave passively during deformation: the validity of this assumption is assessed later.

A sample selected for detailed study was cut parallel to the plane of monoclinic symmetry of the shear zone (i.e. xz-plane of Fig. 1: perpendicular to the shear plane and parallel to the lineation). Particle shapes and orientations were measured on enlarged photographs of the cut surface. The shape of each particle was recorded as R_f = long axis/short axis of the ellipse traced to best match the particle. The orientation, ϕ, was recorded as the angle between the long axis of the ellipse and a reference line (taken as the shear plane). Isogons of the foliation formed by elongation of the feldspar aggregates (Fig. 5) were used to define domains or sub-areas of approximately homogeneous strain, and the strain data was plotted by sub-area. Two examples are shown in Fig. 6. The number of clasts measured in each sub-area ranges from 43 to 93, depending largely on the size of the sub-area.

In order to determine the finite strain ratio, $R_s = (1 + e_1)/(1 + e_2)$ in the plane of observation, marker deformation grids were fitted visually to the data on R_f/ϕ plots (Fig. 6), following the methods proposed by Lisle (1985). R_s values for the four sub-areas range from 3.6 to 8.0, from least deformed outside the main shear zone to most deformed near the center. Note that the highest strains, in the center of the shear zone, could not be determined because the marker particles are ill-defined there.

As a simple check on the values of R_s obtained using the R_f/ϕ method, strains were also estimated by calculation of the harmonic means (Lisle 1977) of the particles in the four sub-areas. Lisle has shown that the harmonic mean is a better estimate of strain than the arithmetic mean or geometric mean. It overestimates the true strain, but its value is within about 10% of R_s for strains larger than $R_s = 2.5$ for a typical sedimentary rock. For the data presented here, the harmonic means compare reasonably well with the values of R_s determined from the R_f/ϕ plots, the difference between the two estimates of strain being no more than 7% (Table 1).

Analysis of strain data

For the purpose of this analysis, we assume that deformation in the shear zone is some combination of variable simple shear, variable volume change, and homogeneous strain (Ramsay & Graham 1970). With this assumption, we seek systematic ways of relating the strains in domains A to D.

Ramsay (1980) showed that the deformation gradient matrix, D, for the deformation resulting from a homogeneous simple shear, γ, followed by a homogeneous volume change, Δ, acting normal to the shear zone boundary is given by:

$$D = \begin{bmatrix} 1 & 0 \\ 0 & 1+\Delta \end{bmatrix} \begin{bmatrix} 1 & \gamma \\ 0 & 1 \end{bmatrix} = \begin{bmatrix} 1 & \gamma \\ 0 & 1+\Delta \end{bmatrix}, \quad (1)$$

where the transformation representing the deformation in xz coordinates is given by:

$$\begin{bmatrix} x' \\ z' \end{bmatrix} = D \begin{bmatrix} x \\ z \end{bmatrix}. \quad (2)$$

The matrix D can be used to find the strain components for varying amounts of shear strain and volume change (e.g. Ramsay & Huber 1983, appendix B).

Assuming that we can determine both shape and orientation of the strain ellipse from the deformed feldspar aggregates, we can plot our data on a graph of orientation, θ', of maximum finite elongation vs strain magnitude, $R = (1 + e_1)/(1 + e_2)$. These may be compared with curves showing variation of θ' with R for different values of volume change, Δ, with increasing shear strain, γ, in an ideal ductile shear zone according to equation (1). This is done in Fig. 7. The data plotted on this graph do not lie along the curve corresponding to $\Delta = 0$, and we conclude that simple shear alone can not account for the observed strain.

The data plotted in Fig. 7 suggest that volume loss increases with increasing strain and that a significant volume loss is associated with the largest strains, near the center of the shear zone. Perhaps surprisingly, the data lie close to a contour of fixed shear strain of about 1.4. This is a possible deformation history. It seems more likely, however, that both shear strain and volume loss developed sympathetically during progressive deformation. We explore this concept in the following. Note that the 'volume loss' referred to here assumes plane strain (no stretch in the y direction) and no strain

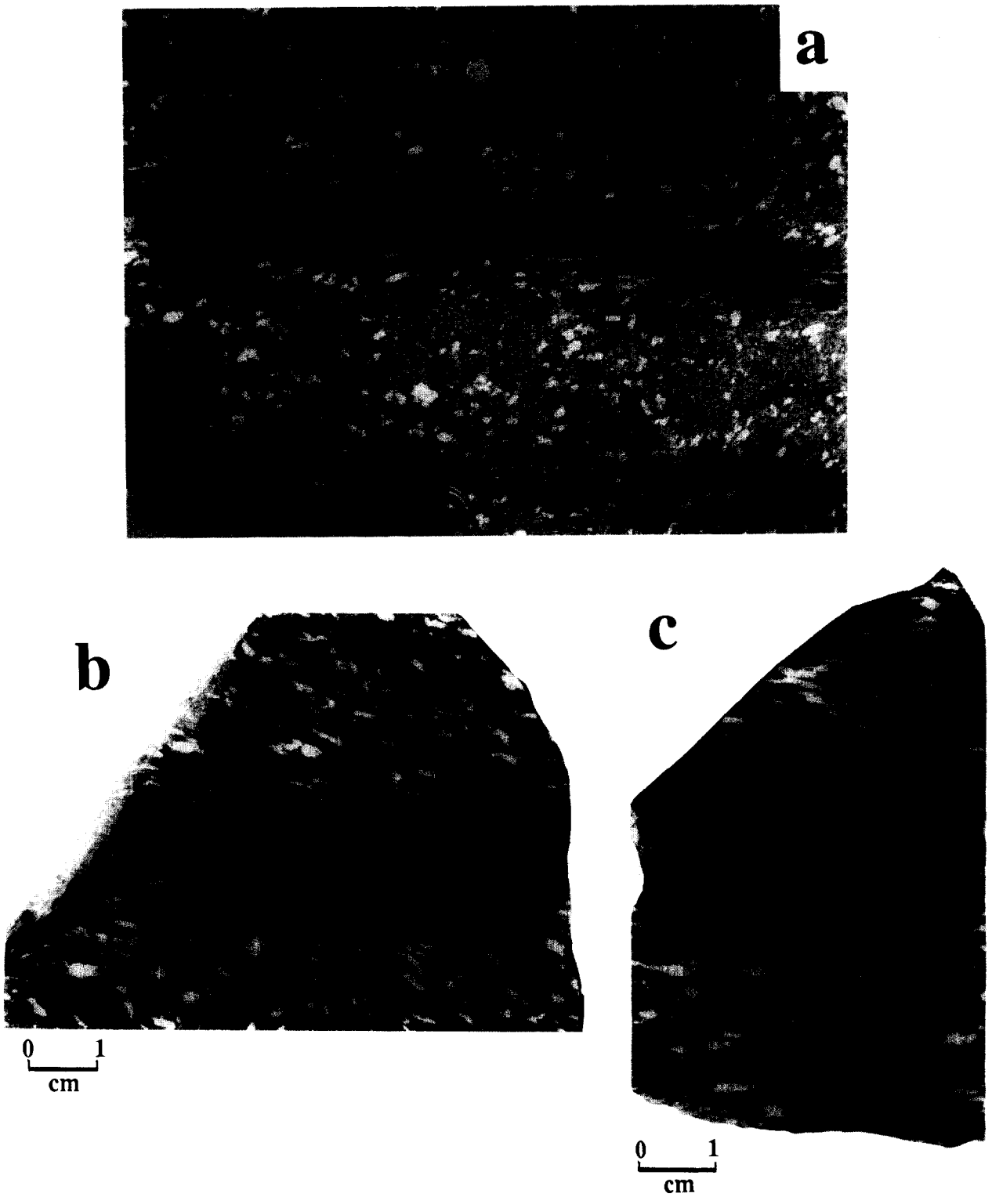

Fig. 3. (a) Field photograph of a shear zone in a section perpendicular to the *xy*-plane, but oblique to *x*. The knife is 10 cm long. (b) Photograph of the selected specimen, cut perpendicular to the shear zone (*xy*-plane) and parallel to the shear direction (*x*). (c) Photogaph of the same sample on a cut (the *yz*-plane) perpendicular to (b).

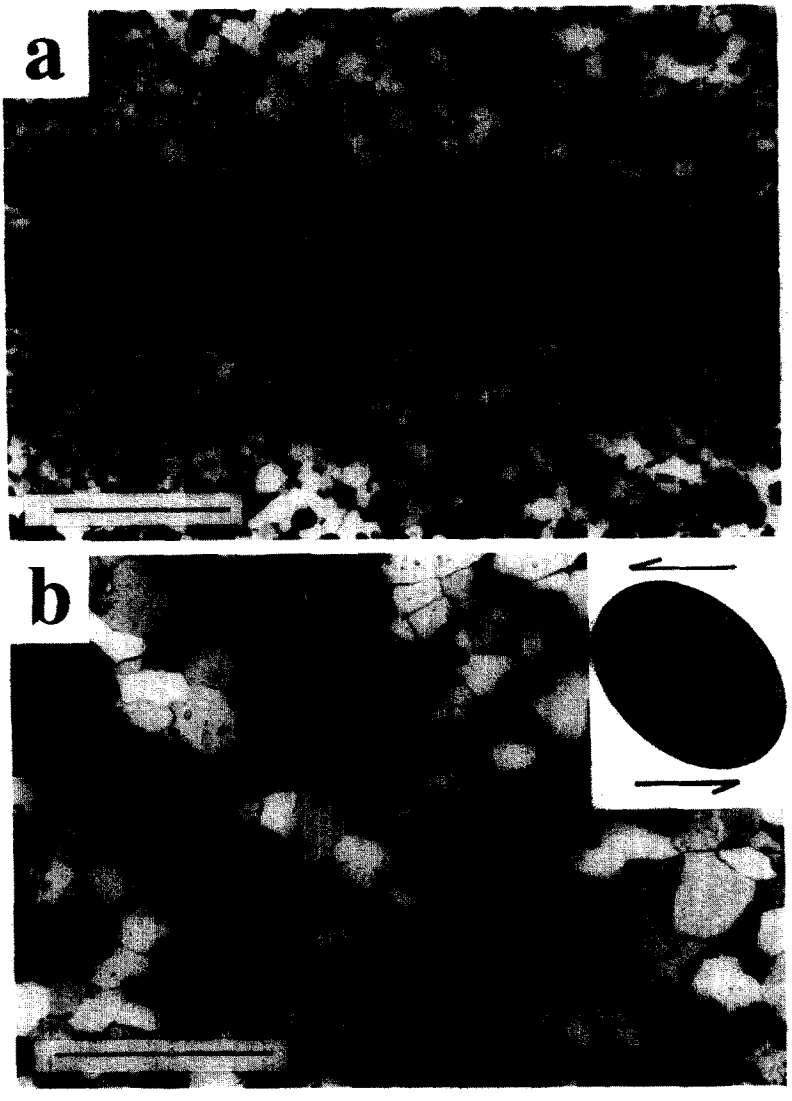

Fig. 4. Photomicrographs of the shear zone in thin sections cut parallel to the face shown in Fig. 3(b): (a) to show bands of different recrystallized grain size parallel to the shear zone bundaries; and (b) to show the shape and orientation of the grain-shape fabric ellipse. In both (a) & (b) the x direction is horizontal. The scale bar is 1 mm in (a) and 0.05 mm in (b).

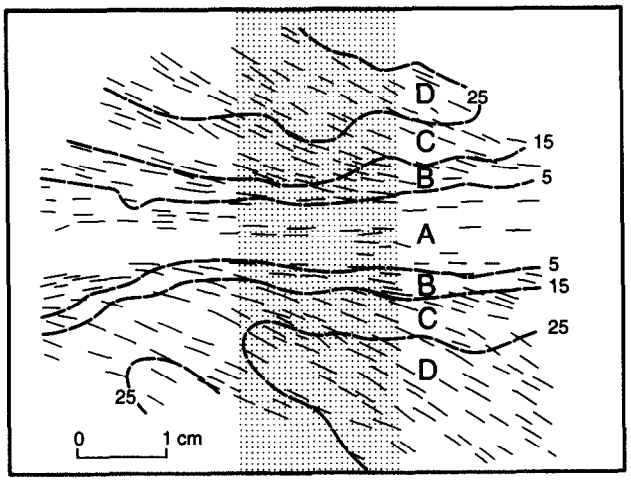

Fig. 5. Isogons of foliation trace (heavy broken lines) at 10° intervals of 'dip' across the shear zone, using the average direction of the shear zone as the reference line (horizontal in this figure). The foliation trace is shown by light discontinuous lines. A, B, C and D are subdivisions of the shear zone, based on the isogons, utilized as domains for strain studies. The stippled area has been used for estimation of volume loss using marker particle size.

outside the shear zone. We can only consider a differential volume loss. There may be in addition a change in volume associated with a homogeneous strain affecting the whole rock; since we do not know the original size of the feldspar aggregates or the phenocrysts that they replace, we can not determine this.

Equations for the simultaneous development of simple shear with volume change perpendicular to the shear zone are presented by Fossen & Tickoff (1993), following the approach of Ramberg (1975). They show that the finite deformation in such a situation is given by:

$$D = \begin{bmatrix} 1 & \dfrac{\gamma\Delta}{\ln(1+\Delta)} \\ 0 & 1+\Delta \end{bmatrix}. \tag{3}$$

Figure 8 is an equivalent plot to Fig. 7, but for simultaneous simple shear with volume change, that is simple shearing (in the sense of Means 1990) and steady rate of volume loss. Note how the contours on this plot differ from those on Fig. 7, and note that the upper off-diagonal element in the deformation matrix differs in equations (1) and (3). The shear strain rate and rate of volume change are constant throughout the deformation represented by equation (3). The strain *path* for this deformation can be followed by multiplying together matrices of equal increments of deformation of arbitrary magnitude. An increment of deformation for simultaneous simple shear and volume change corresponding to the finite deformation of equation (3) is given by:

$$D_{\text{inc}} = \begin{bmatrix} 1 & -\dfrac{\gamma}{n}\dfrac{1-(1+\Delta)^{1/n}}{\ln(1+\Delta)^{1/n}} \\ 0 & (1+\Delta)^{1/n} \end{bmatrix}, \tag{4}$$

where n is the number of increments. This equation can be found from equations (7) and (13) of Fossen & Tikoff (1993). Note that $D = D_{\text{inc}}^{n}$.

The values of θ' and R for zone A, in which the largest strains in the shear zone are recorded, correspond approximately to values of γ and Δ of 1.4 and -0.85, respectively (Fig. 8). By substituting these values into equation (3), we obtain the total deformation matrix:

$$D = \begin{bmatrix} 1 & 0.627 \\ 0 & 0.15 \end{bmatrix}, \tag{5}$$

and taking for convenience $n = 10$ and substituting for γ and Δ into equation (4), we arrive at the incremental deformation matrix:

$$D_{\text{inc}} = \begin{bmatrix} 1 & 0.128 \\ 0 & 0.827 \end{bmatrix}. \tag{6}$$

We can use these to find the path of constant ratio of shear strain rate to rate of volume change that will result in a total strain equal to that recorded in zone A. This is

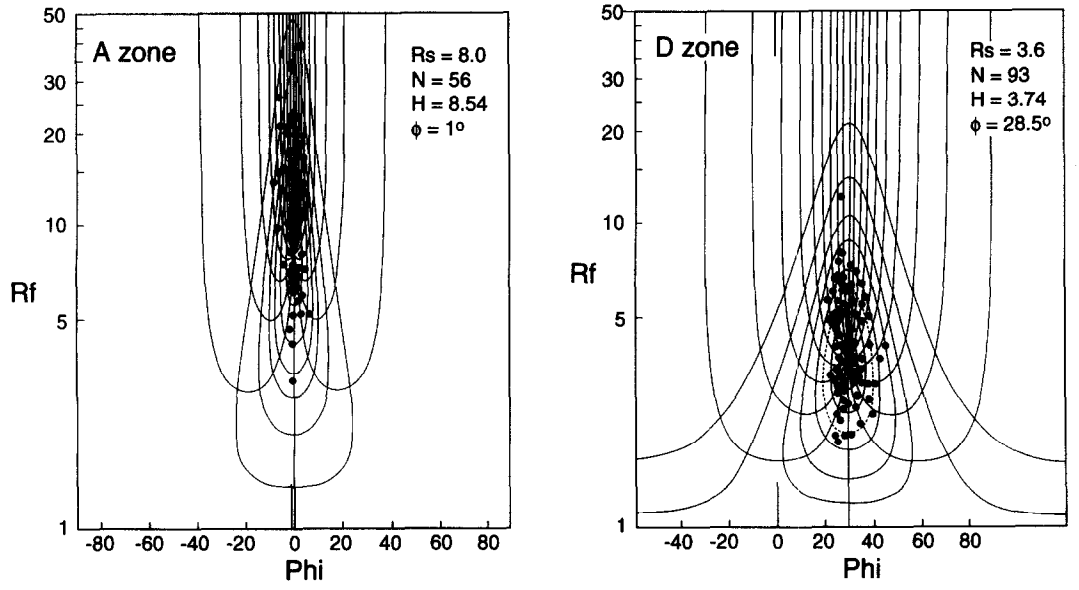

Fig. 6. R_f/ϕ plots (after Lisle 1985) of deformed feldspar aggregates for the most and least deformed domains of the shear zone. R_s = Strain ratio; N = Number of particles measured; H = Harmonic mean; ϕ = angle between the shear zone boundary (x-direction) and the long axes of the feldspar aggregates.

Table 1. Strain data for the shear zone shown in Fig. 3(b), subdivided according to the divisions shown in Fig. 5. N is the number of particles measured, R_s and ϕ the strain ratio and orientation of the long axis of the strain ellipse derived from using the R_f/ϕ method. H is the harmonic mean of the particle shapes. 'Area' is the average area of marker particles in each zone as measured on the photographs. 'Vol. loss' is the loss in volume in each zone assuming zone D is the reference state and loss affects markers and matrix uniformly

Zone	N	R_s	ϕ	H	Difference between R_s and H $(H - R_s)/H \times 100$	Average particle area (mm^2)	Vol. loss
A	56	8.00	1.0	8.54	−6.8%	20.1	75%
B	43	6.50	12.0	6.67	−2.8%	47.4	41%
C	91	4.60	18.0	4.76	−3.5%	56.8	30%
D	93	3.60	28.5	3.74	−4.1%	81.4	0%

shown as path a on Fig. 8 (note that although a is calculated as a steady-state deformation path, it will also be the path followed if $\dot{\gamma}$ and $\dot{\Delta}$ vary in time, but the ratio $\dot{\gamma}/\dot{\Delta}$ remains fixed). It is apparent that this strain path can not account for deformation across the shear zone as a whole. We can generalize this to state that no path consisting of simple shear and volume loss in constant proportions can account for the data. All such paths will be approximately parallel to path a and the path for true simple shear ($\Delta = 0$).

An alternative attempt to find a possible deformation path to account for the data is to take the least deformed state as a starting point and the most deformed state as the end point, and to find a path of constant strain increments that connects the two. The least deformed state (zone D) corresponds approximately to values of γ and Δ of 1.4 and 0.0, respectively (Fig. 8). If D_o and D_f represent deformation matrices for initial and final states, the deformation D_i that connects the two can be found from:

$$D_f = D_i D_o.$$

or

$$\begin{bmatrix} 1 & 0.627 \\ 0 & 0.15 \end{bmatrix} = \begin{bmatrix} 1 & k_1 \\ 0 & k_2 \end{bmatrix} \begin{bmatrix} 1 & 1.4 \\ 0 & 1.0 \end{bmatrix}. \quad (7)$$

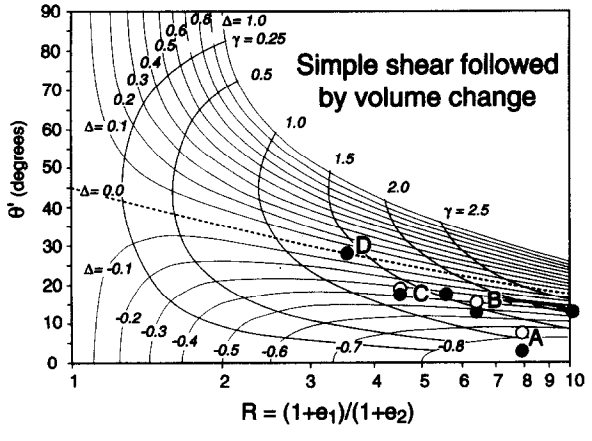

Fig. 7. Theoretical plot showing relationship between strain magnitude, $R = (1 + e_1)/(1 + e_2)$, and orientation of maximum stretch, θ', for simple shear of magnitude γ followed by homogeneous volume change Δ (after Ramsay & Huber 1983, fig. 3.20). Solid circles = data (from Fig. 6 or Table 1) for the four subdivisions of the shear zone. Open circles = plot of volume change (determined from size of the feldspar aggregates—Table 1) against R for shear zone subdivisions A–C. Shaded circles = plot of volume change against ϕ for shear xone subdivisions B and C.

From this it can be found that $k_1 = -0.773$ and $k_2 = 0.15$. The matrix

$$D_i = \begin{bmatrix} 1 & -0.773 \\ 0 & 0.15 \end{bmatrix} \quad (8)$$

is a deformation involving simple shear and volume change only. We can find the steady-state path that results in the deformation given by D_i by multiplying together matrices of incremental strains as before, taking D_o as the starting point. The result is path b on Fig. 8. This is not a good fit to the data and, strikingly, it involves simple shear components of *opposite* sense to that leading to the strain in zone D. In other words, we have a shear zone in which the initial deformation is uniform simple shear (with $\gamma = 1.4$) and, say, dextral in sense, and this is followed by further simple shear of *sinistral* sense, now accompanied by volume loss. This additional strain proceeds to higher intensities towards the center of the shear zone and, interestingly, continues to lead to cumulative strains that increase in axial ratio consistent with dextral shear. This scenario seems very unlikely, as there is no evidence from the rock or thin section to suggest any reversal in the sense of shear.

Deformation path b on Fig. 8 appears to follow a contour of constant γ. This is misleading in that this contour represents constant γ only for those deformations following paths parallel to a (i.e. with a constant ratio of shear strain rate to rate of volume loss). The deformation along a path that starts at the least de-

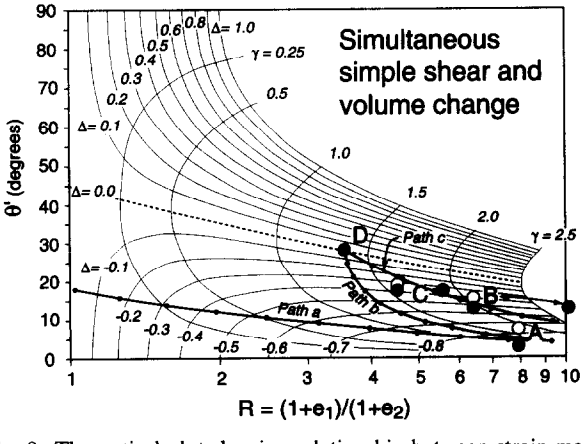

Fig. 8. Theoretical plot showing relationship between strain magnitude, R, and orientation, θ', for simultaneous simple shearing and volume change (after Fossen & Tikoff 1993). Open, shaded and solid circles as in Fig. 7. The small solid circles connected by three different lines trace out model strain paths, as labeled. See text for explanation.

formed state (zone D) and continues with volume loss alone is given at any stage by:

$$D = \begin{bmatrix} 1 & 0 \\ 0 & 1+\Delta_i \end{bmatrix}^n \begin{bmatrix} 1 & 1.4 \\ 0 & 1.0 \end{bmatrix}, \quad (9)$$

where Δ_i is an increment of volume loss of arbitrary size and n is the number of increments. This is plotted as path c on Fig. 8. It is equal to the contour given by $\gamma = 1.4$ on Fig. 7. This path, although not a good fit, is a somewhat better match to the data than paths a or b.

In a continued search for simple deformation paths that might satisfy the data, we should consider those for which there is a homogeneous strain affecting both wall rock and shear zone and either pre-existing or post-dating the development of the shear zone, noting that for the sample analyzed, there are no undeformed regions outside the zone of focused shear. It is not possible to have a *steady state* path of synchronous simple shear, volume loss and homogeneous strain [for which equations equivalent to (3) and (4) can be written, Fossen & Tikoff 1993], active for different lengths of time across the zone, because only simple shear and volume loss can vary continuously across a shear zone and maintain geometric compatibility. One can not have a gradient in a general homogeneous strain without having a gradient in stretch parallel to the shear zone, a violation of shear zone band geometry.

The simplest case of a *pre-existing* homogeneous strain has, in effect, already been considered (path b) for which the pre-existing strain is equal to the strain recorded in the least deformed domain. This strain was taken to be a simple shear with no volume change in equation (7), but it could equally well have been a coaxial or more general strain involving rotation. The nature of the strain in domain D does not affect the arguments about the *subsequent* steady-state strain paths (b or c, Fig. 8) that take the strain in domain D as the starting point. More general preexisting homogeneous strains could be considered, but it is not possible, we believe, to find one from which the strains recorded in each of domains A through D could be produced by a steady-state flow involving simple shear and volume loss.

Turning to the case of a homogeneous strain *following* development of the shear zone, we treat it in the following way. Within a domain of the shear zone in which the strain can be taken to be homogeneous, let the observed strain be given by deformation matrix, D_{obs}. This depends on the state of strain due to shear zone development, D_{sz}, and the superimposed strain, D_h, according to

$$D_{obs} = D_h D_{sz}. \quad (10)$$

The shear zone strain, D_{sz}, is thus

$$D_{sz} = D_h^{-1} D_{obs}. \quad (11)$$

The simplest situation is the one in which the homogeneous strain is equivalent to the lowest strain recorded—that in domain D in our case. The problem is then one of removing the effects of the strain in domain D from the recorded strains in the other domains. For this purpose, the unknown rotations and volume changes associated with these deformations can be ignored, and equation (10) for domain C, for example, can be written as

$$\begin{bmatrix} a_C & b_C \\ b_C & d_C \end{bmatrix} = \begin{bmatrix} a_D & b_D \\ b_D & d_D \end{bmatrix} \begin{bmatrix} a_{szC} & b_{szC} \\ c_{szC} & d_{szC} \end{bmatrix}, \quad (12)$$

and equation (11) as

$$\begin{bmatrix} a_{szC} & b_{szC} \\ c_{szC} & d_{szC} \end{bmatrix} = \frac{1}{(a_D d_D - b_D^2)} \begin{bmatrix} d_D & -b_D \\ -b_D & a_D \end{bmatrix} \begin{bmatrix} a_C & b_C \\ b_C & d_C \end{bmatrix}. \quad (13)$$

The elements of the matrices on the right hand side of equation (13) can be found from the measured axial ratios and orientations of the strains in each domain. For any domain, N, we have

$$\begin{bmatrix} a_N & b_N \\ b_N & d_N \end{bmatrix} = \begin{bmatrix} \cos\theta' & \sin\theta' \\ -\sin\theta' & \cos\theta' \end{bmatrix} \begin{bmatrix} R^{1/2} & 0 \\ 0 & R^{-1/2} \end{bmatrix} \cdot \begin{bmatrix} \cos\theta' & -\sin\theta' \\ \sin\theta' & \cos\theta' \end{bmatrix}. \quad (14)$$

The results of removing, in this way, the strain in domain D from the strains in the other domains is shown in Table 2. Note that to find the orientations of the principal stretches of the 'remnant' strain, D_{sz}, with respect to the shear zone boundaries, we must take into account the reorientation of the shear zone itself by the superposed strain, D_h. To do this we subtract the value of θ' of the remnant strains in each domain from the angle (35°) the shear zone makes with the x-axis after the superposed strain is removed. The results are tabulated in Table 2. The values of R and θ' for the remnant strains in domains A–C are plotted in Fig. 9. We can see that the data are more consistent with a steady state strain path of simple shear and volume loss, that is a path parallel to a, than the original strain data for the three domains (cf. Figs. 8 and 9).

The volume losses considered above are inferred from Figs. 7, 8 and 9 but they can also be measured independently if we assume that the average size of the feldspar aggregates was originally the same across the shear zone. The areas of individual aggregates were measured in a traverse across the shear zone, shown in Fig. 5, to cover all four domains of aggregate preferred orientation. Area of an individual aggregate was recorded as length times breadth, and the average area in each domain was calculated. The domain, D, of least deformation was taken as the reference state, and the average

Table 2. 'Residual' strains, R, in zones A, B and C found by removing the strain measured in zone D from the strains in zones A–C given in Table 1

Zone	R	φ
A′	7.85	3.1°
B′	3.45	13.0°
C′	1.82	18.6°

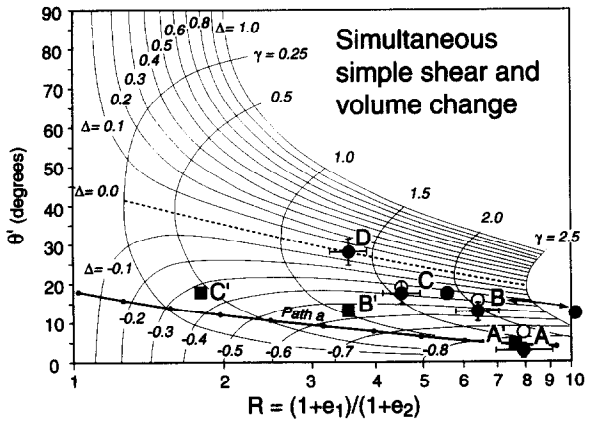

Fig. 9. The same plot as Fig. 8, minus strain paths *b* and *c* and with the residual strains in domains A, B and C added (solid squares). Error bars have also been added to the points representing the original strain data (see text for explanation).

areas of the aggregates in the other domains were normalized by dividing by the average area of the aggregates in domain D. The resulting normalized area can be expressed as a volume change, D, and this is given in Table 1 and plotted as functions of both R and ϕ in Figs. 7, 8 and 9. In these figures, the data are consistent with the data on clast shape and orientation if R is fixed, but not if ϕ is fixed. In either case, if monoclinic symmetry is maintained (and differential flow in y disallowed), they indicate progressive volume loss towards the center of the shear zone.

Overall, the geometric data are consistent with increasing volume loss towards the center of the shear zone. They do not support a model involving a deformation path with a constant ratio of shear strain rate to rate of volume loss. They are more compatible with a path of simple shear followed by progressive volume loss, or with a path consisting of simple shearing and rate of volume loss in constant proportions followed by a homogeneous strain (equal to the strain in domain D) affecting the whole rock. The data do not allow any assessment of the way the shear zone developed with time—that is did it start as a narrow, short perturbation and grow wider and longer, or did it develop its full dimensions early, and strain become progressively focused on a narrower zone with time?

No consideration in the above analysis was given to strain in the third dimension. To the extent that the shear zone has monoclinic symmetry, the strain in y (Figs. 1 and 3c) has no influence on the analysis, except that a (uniform) stretch in y would imply a commensurate uniform change in area in the xz-plane. The strain in y could be acquired at any time in any of the various scenarios discussed above, and deformation paths involving constant proportions of simple shearing, $\dot{\gamma}$, to volume loss rate, $\dot{\Delta}$, to rate of stretching in y, $\dot{e}_y$, are conceivable. Extending the conclusions of the last paragraph to three-dimensions, however, such a path could only explain the data if $\dot{\gamma}$, $\dot{\Delta}$ and $\dot{e}_y$ in constant proportions are followed by a homogeneous strain equivalent to the strain in domain D in the xz-plane.

GEOCHEMICAL ANALYSIS

Another way of studying volume change accompanying various processes in rocks is by comparing the chemical composition of the region in which volume change is suspected with the composition of the rock outside. In practice, the comparison is based on a hypothetical representative element volume (REV) of each subspace of interest that defines the average grain density of the rock. Intergranular pore space and other voids are not included in the REV, only the packing of atoms in the constituent minerals is considered.

Whole-rock geochemical analyses were performed on several samples from the shear zone and from outside the shear zone (the 'wall rock'), and the results are presented in Table 4 and plotted in Fig. 10. (It should be noted that these samples cannot be equated directly with the domains defined above for the strain analysis.) The whole rock compositions shown in Table 4 were determined by Inductively Coupled Plasma Mass Spectrometry (ICPMS) after lithium metaborate fusion and acid digestion of the rock powders (<100 μm).

Figure 10 is an isocon diagram (Grant 1986) comparing the composition of sample 2 within the shear zone (in the region of highest strain) to that of sample 6 within the wall rock (region of lowest strain), and its construction is based on the method of Gresens (1967) for analysis of the changes in volumes and concentrations of minerals and elements during metasomatism. The principle is based on the knowledge that during metasomatism, or other geological processes involving introduction or removal of material, the mobility of elements will differ, and in particular, immobile elements will all have the same ratio of concentration in the original (C_o) to their concentration in the altered (C_a) rock. Such elements will plot on a straight line through the origin on an isocon diagram.

Most interestingly, the data plotted in Fig. 10 do not depart greatly from the constant mass line ($C_o = C_a$), or from the constant volume line ($C_o\rho_o = C_a\rho_a$), where ρ_o and ρ_a are the average grain densities in the wall rock and shear zone, respectively, determined from the weighted densities of the minerals in the rock (see the modal analysis of the rock in Table 3). Except for K, P and Ce, all elements lie within the region defined by

Table 3. Modal analysis of minerals in the shear zone margins (wall rock) and in the shear zone, expressed as area (and assumed volume) per cent

Mineral	Margin	Shear zone
Sphene*	1.2	0.1
Diopside	6.6	1.1
Quartz	20.9	18.4
Muscovite	1.6	0.8
Hematite	0.1	0
Clinozoisite	1.5	0.1
Plagioclase (AnX)	8.1	9.1
Hornblende	44.5	58.0
Tourmaline	0.1	0
Garnet	15.4	12.4

*Altered to leucoxene and calcite.

Table 4. Composition of selected volumes within the amphibolite shear zone and in the adjacent wall rock. Samples 1 and 2 are from the center of the shear zone (equivalent to zone A of Fig. 5), samples 3 and 4 represent moderate strain samples at the border of the shear zone (equivalent to zones C and D of Fig. 5), and sample 6 is from a low strain zone about 5 cm from the center of the shear zone. Whole-rock ICPMS analyses

	Sample no. 1	$\sigma(\pm)$	Sample no. 2	$\sigma(\pm)$	Sample no. 3	$\sigma(\pm)$	Sample no. 4	$\sigma(\pm)$	Sample no. 6	$\sigma(\pm)$
Majors, wt%										
SiO_2	50.97	0.64	50.84	0.30	51.31	0.59	51.76	0.86	52.66	0.55
TiO_2	1.06	0.01	1.23	0.01	1.02	0.01	1.06	0.01	0.82	0.01
Al_2O_3	16.85	0.11	16.63	0.16	17.49	0.15	18.23	0.29	18.56	0.20
Fe_2O_3 (Total)	10.96	0.09	11.20	0.10	9.62	0.03	9.52	0.04	9.30	0.05
MnO	0.21	0.00	0.21	0.00	0.17	0.00	0.17	0.00	0.17	0.00
MgO	6.38	0.08	6.40	0.05	6.35	0.05	6.21	0.06	6.01	0.08
CaO	11.71	0.01	11.69	0.12	11.94	0.08	12.23	0.11	11.38	0.11
Na_2O	3.03	0.03	3.45	0.04	2.83	0.05	2.61	0.05	2.64	0.04
K_2O	0.35	0.01	0.59	0.01	0.31	0.01	0.29	0.01	0.27	0.01
P_2O_5	0.08	0.01	0.06	0.01	0.07	0.00	0.07	0.00	0.10	0.01
Total	101.56	0.99	102.30	0.81	101.11	0.96	102.16	1.42	101.89	1.06
Trace Elements, ppm										
Sr	210.97	1.35	209.50	2.17	222.83	2.90	237.60	3.04	252.06	4.29
Y	17.08	0.13	16.51	0.18	17.32	0.18	16.49	0.14	17.3	0.11
Ba	88.10	1.06	103.68	1.92	100.08	0.89	96.97	2.66	119.61	2.47
La	6.75	0.10	7.55	0.11	6.97	0.08	6.17	0.10	9.21	0.06
Ce	16.22	0.07	15.01	0.15	16.40	0.15	15.13	0.21	21.33	0.21
Pr	2.25	0.03	2.07	0.02	2.23	0.04	2.03	0.04	2.86	0.04
Nd	10.07	0.12	9.26	0.15	10.14	0.24	9.12	0.19	12.54	0.16
Sm	2.70	0.10	2.53	0.06	2.74	0.06	2.53	0.06	3.16	0.07
Eu	0.99	0.02	0.97	0.03	0.96	0.03	0.91	0.02	1.24	0.02
Gd	3.03	0.07	2.95	0.12	3.10	0.11	2.91	0.07	3.34	0.08
Tb	0.53	0.01	0.50	0.01	0.54	0.01	0.51	0.01	0.56	0.01
Dy	3.38	0.05	3.12	0.03	3.36	0.10	3.12	0.08	3.39	0.12
Ho	0.68	0.01	0.65	0.02	0.69	0.01	0.65	0.03	0.70	0.02
Er	1.93	0.07	1.86	0.03	1.93	0.02	1.85	0.02	1.96	0.05
Tm	0.28	0.01	0.28	0.01	0.28	0.01	0.26	0.01	0.28	0.01
Yb	1.80	0.04	1.75	0.03	1.84	0.06	1.73	0.04	1.92	0.03
Lu	0.29	0.01	0.28	0.01	0.27	0.02	0.28	0.01	0.31	0.01

constant mass loss/gain rays extending through Ti and Nd. In general, Ti and rare earth elements (REE) like Nd are considered to be relatively immobile elements during metamorphism (e.g. Knoper & Condie 1988). If Ti had remained immobile during deformation, a volume decrease within the shear zone of 30% would be implied; if Nd had remained immobile, a volume increase of 30% would be implied.

The actual change in volume is probably considerably less than 30% because other immobile elements like Y and Al are very close to the line of constant volume (and constant mass). Some elements like Ti, while relatively immobile, reside predominantly in refractory phases (e.g. rutile) that may be difficult to dissolve in preparation for whole rock chemical analysis. Therefore the analytical precision of Ti may be suspect. In addition, the relative mobility of the REE during metamorphic processes is not well known (Grauch 1989). Because so many elements lie close to the constant mass or constant volume lines on Fig. 10, the true change in volume within the shear zone, compared with the wall rock, that occurred as a result of metamorphic and deformational processes is probably less than 15%, assuming that chemical equilibration subsequent to deformation has not occurred.

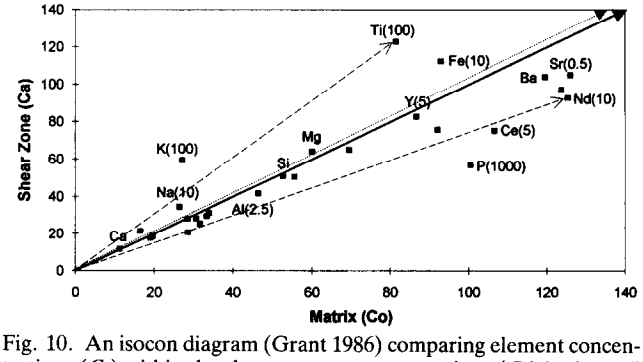

Fig. 10. An isocon diagram (Grant 1986) comparing element concentrations (C_a) within the shear zone to concentrations (C_o) in the wall rock, using the data given in Table 4, for samples 2 and 6. Element labels and scaling factors (in parentheses) for major elements (oxide wt% units) and selected trace elements (ppm) are provided. The slope of the line of constant volume ($C_o\rho_o = C_a\rho_a$, short dashed arrow) is approximately 5% steeper than the slope of the line of constant mass ($C_o = C_a$, solid arrow). With the exception of K, P and Ce, the concentrations of the major components, Sr, Ba and REE are within the region defined by the long-dashed arrows to Ti and Nd (see text for explanation).

It should be noted that other isocon plots of selected samples from Table 4 show even less deviation from the constant volume line or constant mass line than Fig. 10, strengthening the argument against significant volume changes associated with metamorphism and deformation in these shear zones. Overall, the geochemical data permit about a 15% loss in volume in the shear zone, but not the very large losses implied by the geometric analysis.

DISCUSSION

In the geometric analysis, we have not considered errors in the measurements of the shape, size and

orientation of the feldspar aggregates, and in the fitting of R_f/ϕ curves to the data. These are not easy to assess. The aggregates are irregular in shape and can only roughly be approximated by ellipses on the cut section. Repeated measurements on three individual particles gave ranges in R of ln 1.55 ± 0.19, 1.05 ± 0.19, and 1.60 ± 0.22 and in ϕ of 3.63 ± 0.08, 2.89 ± 0.37 and 3.17 ± 0.29, respectively. Because of (i) the errors in measurement and in representing the particles as ellipses, (ii) the gradient of strain across the shear zone, and (iii) the limited number of particles within each 'homogeneous' domain across the shear zone, there are quite large uncertainties in the fitting of R_f/ϕ curves to the data (Fig. 6), and in assigning 'average' strains to domains A–D. It seems reasonable, however, that fitted curves in the range ln $R = 0.1$–0.15 and $\phi = 5°$ will accommodate these errors, and 'error bars' of these amounts are shown on Fig. 9. Errors in ϕ decrease as R increases, and in the center of the shear zone the error in ϕ is estimated at 2°.

The potential existence of a primary fabric of preferred shape and orientation of the feldspar aggregates can not be ruled out, and would be geometrically equivalent to a pre-existing strain. The simplest case of such a fabric would be if the recorded 'strain' in the outermost domain, D, were entirely due to such a fabric. Elsewhere in these metagabbros, regions away from the shear zones show little evidence of preferred orientation of feldspar aggregates, and so anything but a weak primary fabric or pre-existing strain seems unlikely. The bulk stretch in y, noted in the shear zone sample analyzed in detail (Fig. 3), also does not appear to be regional in development.

In measuring strain in the rock, it is assumed that the feldspar aggregates deform homogeneously with the matrix. There is no curving of foliation around or boudinaging of the aggregates to suggest they are stiffer than the matrix, nor are there any local cusps in the interfaces between aggregates and matrix to suggest a difference in competence. In addition, the shape fabric of the recrystallized grains is similar inside and outside the aggregates. All these suggest that differences in competence of aggregate and matrix are small.

It is clear from measurements and from Fig. 3 that the aggregates become smaller towards the center of the shear zone, and in fact they can not be distinguished at all in a central strip about 7 mm wide. It seems likely that dynamic recrystallization in such a highly deformed rock is an agent of 'mixing', by progressive new grain growth, grain rotation, grain-boundary slip and nearest-neighbor swapping. These will act as a kind of diffusive process of homogenization and may cause the feldspar aggregates to shrink, without necessarily any net volume loss. These processes of 'attrition' will be most effective in removing grains from the ends of the stretched aggregates, where they are thinnest. Thus it seems likely that the aspect ratios of the feldspar aggregates, and thus strain, is underestimated and volume loss (based on size) overestimated. This effect will be significant in domain A, but is likely to be much less marked in the other domains, because in these the edges of the aggregates are sharply defined. It may account for the point representing domain A in Fig. 8 lying off the trend defined by the (admittedly only three) other points. The sense of offset of the point from this trend is consistent with this interpretation.

Attrition of the ends of the aggregates, by the processes just described, exaggerates the apparent volume loss, but by itself can not account for more than about 30% of it (this figure is computed by assuming all the 'lost' material is taken from the ends of the aggregates, thus shrinking them and reducing their aspect ratio). Taken together, the data on *shape* and *orientation* of the aggregates and on the *size* of the aggregates (Figs. 8 and 9) indicate at least significant loss of *area* in the plane perpendicular to the shear zone and parallel to the shear direction. The data also suggest that this loss of area affects the whole rock and is not selective removal of feldspar from the aggregates. If it were the latter, apparent area loss due to shrinking of the size of the aggregates (a 'local' effect) would be greater than the apparent area loss deduced from the shape and orientation of the aggregates (a 'global' effect).

So far unquestioned in this discussion is the underlying assumption of the band structure of the shear zone. As stated in the introduction, the argument that strain must be a combination of simple shear plus volume change stems from this assumption (Ramsay & Graham 1970). Although the isogons of foliation trace are subparallel, there is some variation in the width of the shear zone across the selected sample (see Fig. 5), indicating that there must be a strain gradient along the shear zone. Also, some narrowing of the shear zone across the sample can be seen in the yz plane (Fig. 3c), indicating a deviation from monoclinic symmetry. It is not clear whether these changes in width of the shear zone in the two sections are large enough to account for gross deviations from simple shear ± volume loss. The average length of the feldspar aggregates in the y direction, as seen in the yz section (Fig. 3c), is almost the same inside and outside the shear zone. There is thus little evidence from particle shape for differential flow of material in the y direction.

Domains of localized shear are often arranged in a three-dimensional network (e.g. Ramsay & Allison 1979, Bell 1981, Choukroune & Gapais 1983), the pattern of which seems to depend on the bulk strain and bulk kinematics of the rock (Gapais *et al.* 1987). There is certainly evidence of some anastomosing of the shear zones in the amphibolites under investigation, but there is insufficient data to establish if there is any kind of regular pattern. It seems likely that strain within an anastomosing network of shear bands will deviate from the band model, and this may well involve flattening across the shear zones, and lateral extrusion of material around the lozenges of undeformed or weakly deformed rock surrounded by the network of shear zones. Such behavior would lead to true area loss in the plane perpendicular to a shear zone and parallel to the shear direction (xz-plane, Fig. 1), and thus *apparent* volume

Table 5. Average mineral compositions and mineral formulae, determined by microprobe analysis. Standard deviations are in italics. Mineral formulae are normalized to 23, 12, 6 and 8 oxygens for hornblende, garnet, clinopyroxene and plagioclase, respectively

Location	**Marginal zone**										**Shear zone**			
Mineral	Hornblende		Garnet		Clinopyroxene		Plagioclase (pheno.)		Plagioclase (matrix)		Hornblende		Garnet		Plagioclase	
SiO_2	41.36	*0.44*	38.11	*1.03*	52.46	*1.03*	52.68	*5.33*	58.69	*2.09*	41.53	*0.09*	38.38	*0.95*	49.60	*2.65*
TiO_2	1.11	*0.04*	0.05	*0.02*	0.42	*0.68*	0.01	*0.01*	0.01	*0.01*	0.88	*0.06*	0.03	*0.02*	0.00	*0.00*
Al_2O_3	13.93	*0.49*	22.35	*0.32*	1.53	*0.08*	29.16	*3.35*	25.20	*1.02*	14.65	*0.15*	22.51	*0.25*	31.31	*2.21*
MnO	0.02	*0.02*	0.74	*0.09*	0.03	*0.04*	0.02	*0.04*	0.00	*0.01*	0.05	*0.03*	0.59	*0.07*	0.00	*0.00*
FeO	12.27	*0.18*	21.36	*0.56*	6.73	*0.23*	0.06	*0.03*	0.09	*0.07*	13.86	*0.02*	22.32	*0.97*	0.08	*0.02*
MgO	12.14	*0.15*	5.76	*0.06*	15.05	*0.48*	0.02	*0.01*	0.02	*0.01*	11.14	*0.29*	5.85	*0.27*	0.01	*0.02*
CaO	12.01	*0.10*	11.90	*0.30*	23.19	*0.21*	11.82	*4.04*	7.08	*1.22*	11.86	*0.58*	10.80	*0.45*	13.84	*2.57*
Na_2O	1.97	*0.02*	0.02	*0.04*	0.82	*0.08*	5.01	*2.28*	7.92	*0.72*	2.01	*0.22*	0.02	*0.02*	3.75	*1.41*
K_2O	0.83	*0.04*	0.00	*0.00*	0.00	*0.00*	0.09	*0.06*	0.17	*0.04*	0.76	*0.01*	0.00	*0.00*	0.16	*0.20*
Total	95.62	*0.08*	100.28	*1.43*	100.24	*0.88*	98.91	*0.95*	99.19	*0.75*	96.74	*0.57*	100.51	*2.01*	98.75	*0.76*
							Mineral Formulae									
Si	6.230	*0.056*	2.938	*0.040*	1.943	*0.021*	2.411	*0.207*	2.646	*0.067*	6.215	*0.031*	2.950	*0.030*	2.291	*0.120*
Ti	0.126	*0.004*	0.003	*0.001*	0.012	*0.019*	0.000	*0.000*	0.000	*0.000*	0.099	*0.006*	0.002	*0.001*	0.000	*0.000*
Al	2.474	*0.091*	2.031	*0.035*	0.067	*0.003*	1.577	*0.205*	1.340	*0.067*	2.584	*0.023*	2.041	*0.033*	1.704	*0.122*
Mn	0.002	*0.003*	0.048	*0.005*	0.001	*0.001*	0.001	*0.002*	0.000	*0.000*	0.006	*0.004*	0.038	*0.004*	0.000	*0.000*
Fe^{+2}	1.546	*0.026*	1.377	*0.035*	0.209	*0.009*	0.002	*0.001*	0.003	*0.003*	1.735	*0.008*	1.435	*0.047*	0.003	*0.001*
Mg	2.725	*0.028*	0.662	*0.015*	0.831	*0.019*	0.001	*0.001*	0.001	*0.001*	2.487	*0.072*	0.671	*0.027*	0.001	*0.001*
Ca	1.938	*0.014*	0.983	*0.023*	0.920	*0.008*	0.583	*0.207*	0.343	*0.062*	1.902	*0.087*	0.890	*0.036*	0.685	*0.126*
Na	0.575	*0.008*	0.004	*0.006*	0.059	*0.006*	0.443	*0.197*	0.692	*0.056*	0.585	*0.062*	0.004	*0.004*	0.336	*0.126*
K	0.160	*0.007*	0.000	*0.000*	0.000	*0.000*	0.005	*0.003*	0.010	*0.002*	0.146	*0.001*	0.000	*0.000*	0.009	*0.012*
Total	15.774	*0.014*	8.046	*0.024*	4.041	*0.013*	5.024	*0.010*	5.035	*0.008*	15.759	*0.054*	8.030	*0.020*	5.029	*0.021*

loss, when applying the band model to the analysis of strain in the shear zones. This is a possible resolution of the paradox of large volume changes (>80%) implied by the strain analysis and small volume changes (<15%) implied by the geochemical analysis. Removal of mass by bulk flow of rock would be 'invisible' to the isocon analysis.

Having questioned the assumptions inherent in the band model of deformation in a shear zone, we must also question the significance of the isochemical state of the shear zone and its wall rock. The five sub-samples taken for geochemical analysis (Table 4) and the microprobe analysis (Table 5) do indeed show a uniform chemistry and very similar mineralogy from the shear zone to a distance about 5 cm into the wall rock. The consistency of the paleotemperatures and paleopressures across the low strain to high strain volumes of the sample indicates that the entire rock equilibrated at the same conditions during the metamorphic event(s). Furthermore, the isocon analysis indicates that pervasive metasomatism did not occur preferentially along the shear zone. The higher modal abundance of hornblende in the shear zone at the expense of clinopyroxene and garnet (Table 3), however, indicates that the activity of H_2O was probably higher in the shear zone. Therefore the shear zone may have acted as a conduit for fluids during metamorphism. This is not surprising, and there is extensive evidence in other studies for fluids being channelized along shear zones at all crustal levels (e.g. Beach 1976, McCaig 1984, Gilotti 1989, Carter & Dworkin 1990).

It seems unlikely that material loss from a shear zone by dissolution or diffusion can be isochemical, because mineral solubilities and the diffusive mobilities of elements differ. It is, however, possible that chemical segregation did occur during shear zone development and that the isochemical state was attained during annealing after deformation. However, the weak shape fabric (Fig. 4b) consistent with simple shear accompanied by dynamic recrystallization, and the presence of bands of different recrystallized grain size within the shear zone and parallel to the shear zone margins (Fig. 4a), suggests that annealing effects, if any, were slight.

Other studies have encountered the problem of apparent very large volume losses in highly deformed rocks. For example, assuming ductile deformation in a band structure, Mawer (1983) calculated 69–95% volume loss for a quartzite mylonite zone in central Australia, which he suggested was unreasonably high, as there was no other geological evidence indicating that such a large volume loss had occurred. Similarly, Schwerdtner (1982) calculated volume losses of 48–68% in mylonites from the Grenville Front in Ontario, values that he considered unrealistic and perhaps indicative of deficiencies in the band model for shear zones. A similar discrepancy between geometrical evidence for volume loss and geochemical evidence for little or no volume loss exists for shear zones in mobilized basement granitoids in the lower Pennine nappes of the Alps. Assuming immobility of Al_2O_3, Kerrich *et al.* (1977) and Simpson (1983) concluded that there had been little volume loss during shear zone development in part of the Maggia nappe. Recently, Mohanty & Ramsay (1994) presented geometrical evidence, using deformed xenoliths, to indicate that there had been large volume loss in the same shear zones. They reinterpreted the chemical results to conclude that volume losses had occurred, based on immobility of Fe, Mg and Ti, and argued that the geochemical data was consistent with the geometrical evidence.

With the present data, we are unable to unambiguously resolve the inconsistency between geometry and

geochemistry in determining volume loss in the studied shear zones. Further detailed analysis of both the geometry and chemistry of rocks in which localized shear has developed would be rewarding. Such studies should involve determining the full three-dimensional shapes of the shear zones, to determine the deviations from monoclinic symmetry and plane strain, and look at shear zones of different sizes, in which differences in chemistry might be associated with changes in the length scale for diffusion.

Acknowledgements—We thank Neil Mancktelow, Richard Norris and John Watkinson for careful reviews and useful suggestions for improvement of the manuscript. The microprobe analysis was done using the facilities of the U.S. Bureau of Mines in the Twin Cities.

REFERENCES

Andersen, T., Austrheim, H. & Burke, E. A. J. 1991. Mineral–fluid–melt interactions in high-pressure shear zones in the Bergen Arcs nappe complex, Caledonides of W. Norway: implications for the fluid regime in Caledonian eclogite-facies metamorphism. *Lithos* **27**, 187–204.

Armstrong, J. T. 1989. CITZAF: A microprobe/SEM correction program, version 3.03. California Institute of Technology, Pasadena.

Beach, A. 1976. The interrelations of fluid transport, deformation, geochemistry and heat flow in early Proterozoic shear zones in the Lewisian complex. *Phil Trans. R. Soc. Lond.* **A280**, 569–604.

Bell, T. H. 1981. Foliation development: the contribution, geometry and significance of progressive, bulk, inhomogeneous shortening. *Tectonophysics* **75**, 273–296.

Berman, R. G. 1990. Mixing properties of Ca–Mg–Fe–Mn garnets. *Am. Miner.* **75**, 328–344.

Berthé, D., Choukroune, P. & Jagouzo, P. 1979. Orthogneiss mylonite and noncoaxial deformation of granites: the example of the South Armorican Shear Zone. *J. Struct. Geol.* **1**, 31–42.

Burg, J. P. & Laurent, Ph. 1978. Strain analysis of a shear zone in a granodiorite. *Tectonophysics* **47**, 15–42.

Carter, K. E. 1992. Evolution of stacked, ductile shear zones in carbonates from mid-crustal levels: Tuscan nappe, N. Apennines, Italy. *J. Struct. Geol.* **14**, 181–192.

Carter, K. E. & Dworkin, S. I. 1990. Channelized fluid flow through shear zones during fluid-enhanced dynamic recrystallization, northern Apennines, Italy. *Geology* **18**, 720–723.

Choukroune, P. & Gapais, D. 1983. Strain pattern in the Aar granite (Central Alps): orthogneiss developed by bulk inhomogeneous flattening. *J. Struct. Geol.* **5**, 411–418.

Cobbold, P. R. 1977. Description and origin of banded deformation structures. I. Regional strain, local perturbations, and deformation bands. *Can. J. Earth Sci.* **14**, 1721–1731.

Coward, M. P. 1974. Flat lying structures within the Lewisian basement gneiss complex of NW Scotland. *Proc. Geol. Ass.* **85**, 459–472.

Coward, M. P. 1976. Strain within ductile shear zones. *Tectonophysics* **34**, 181–197.

Dipple, G. M., Wintsch, R. P. & Andrews, M. S. 1990. Identification of the scales of differential element mobility in a ductile fault zone. *J. Metam. Geol.* **8**, 645–661.

Etheridge, M. A., Wall, V. J., Cox, S. F. & Vernon, R. H. 1984. High fluid pressures during regional metamorphism and deformation: implications for mass transport and deformation mechanisms. *J. geophys. Res.* **89**, 4344–4358.

Fossen, H. & Tikoff, B. 1993. The deformation matrix for simultaneous pure shear, simple shear, and volume change, and its implications to transpression/transtension tectonics. *J. Struct. Geol.* **15**, 413–422.

Gapais, D., Bale, P., Choukroune, P., Cobbold, P. R., Mahjoub, Y. & Marquer, D. 1987. Bulk kinematics from shear zone patterns: some field examples. *J. Struct. Geol.* **9**, 635–646.

Gates, A. E. & Speer, J. A. 1991. Allochemical retrograde metamorphism in shear zones: an example in metapelites, Virginia, U.S.A. *J. Metam. Geol.* **9**, 581–604.

Gee, D. G. & Zachrisson, E. 1979. The Caledonides in Sweden. *Sver. geol. Unders.* C **769**.

Gilotti, J. A. 1989. Reaction progress during mylonitization of basaltic dikes along the Särv thrust, Swedish Caledonides. *Contrib. Mineral. Petrol.* **101**, 30–45.

Glazner, A. F. & Bartley, J. M. 1991. Volume loss, fluid flow and state of strain in extensional mylonites from the central Mojave Desert, California. *J. Struct. Geol.* **13**, 587–594.

Graham, C. M. & Powell, R. 1984. A garnet–hornblende geothermometer: calibration, testing, and application to the Pelona Schist, Southern California. *J. Metam. Geol.* **2**, 13–31.

Grant, J. A. 1986. The isocon diagram—a simple solution to Gresens' equation for metasomatic alteration. *Econ. Geol.* **81**, 1976–1982.

Grauch, R. I. 1989. Rare earth elements in metamorphic rocks. In: *Geochemistry and Mineralogy of Rare Earth Elements* (edited by Lipin, B. R. & McKay, G. A.). *Reviews in Mineralogy* **21**, 147–161.

Gresens, R. L. 1967. Composition-volume relationships for metasomatism. *Chem. Geol.* **2**, 47–55.

Hanmer, S. 1986. Asymmetrical pull-aparts and foliation fish as kinematic indicators. *J. Struct. Geol.* **8**, 111–122.

Hara, I., Takeda, K. & Kimura, T. 1973. Preferred lattice orientation of quartz in shear deformation. *Hiroshima Univ. J. Sci. Ser.* **C7**, 1–10.

Hudleston, P. J. 1977. Progressive deformation and development of fabric across zones of shear in glacial ice. In: *Energetics of Geological Processes* (edited by Saxena, S. & Bhattacharji, S.). Springer-Verlag, New York, 121–187.

Kerrich, R., Fyfe, W. S., Gorman, B. E. & Allison, I. 1977. Local modification of rock chemistry by deformation. *Contrib. Mineral. Petrol.* **65**, 183–190.

Knoper, M. W. & Condie, K. C. 1988. Geochemistry and petrogenesis of early Proterozoic amphibolites, west-central Colorado, U.S.A. *Chem. Geol.* **67**, 209–225.

Kohn, M. J. & Spear, F. S. 1989. Empirical calibration of geobarometers for the assemblage garnet + hornblende + plagioclase + quartz. *Am. Mineral.* **74**, 77–84.

Kulling, O. 1964. Översikt över norra Norrbottensfjällens Kaledonberggrund. *Sver. geol. Unders.*, Ba **19**.

Lin, S. & Williams, P. F. 1992. The geometrical relationship between the stretching lineation and the movement direction of shear zones. *J. Struct. Geol.* **14**, 491–497.

Lisle, R. J. 1977. Estimation of tectonic strain ratio from the mean shape of deformed elliptical markers. *Geol. Mijnb.* **56**, 140–144.

Lisle, R. J. 1985. *Geological Strain Analysis. A Manual for the R_f/ϕ technique*. Pergamon Press, Oxford.

Lister, G. S. & Snoke, A. W. 1984. S–C mylonites. *J. Struct. Geol.* **6**, 617–638.

Lister, G. S. & Williams, P. F. 1979. Fabric development in shear zones: theoretical controls and observed phenomena. *J. Struct. Geol.* **1**, 283–297.

Lloyd, G. E., Law, R. D., Mainprice, D. & Wheeler, J. 1992. Microstructural and crystal fabric evolution during shear zone formation. *J. Struct. Geol.* **14**, 1079–1100.

Mawer, C. K. 1983. State of strain in a quartzite mylonite, Central Australia. *J. Struct. Geol.* **5**, 401–409.

McCaig, A. M. 1984. Fluid–rock interaction in some shear zones from the Pyrenees. *J. Metam. Geol.* **2**, 129–141.

Means, W. D. 1990. Review paper—kinematics, stress, deformation and material behavior. *J. Struct. Geol.* **12**, 953–971.

Mitra, G. 1975. Shear zones and mylonites: a look at the mechanical processes involved in the deformation of basement (abstract). *Geol. Soc. Am. Abstr. Progr.* **7**, 1202–1203.

Mitra, G. 1978. Ductile deformation zones and mylonites: the mechanical processes involved in the deformation of crystalline basement rocks. *Am. J. Sci.* **278**, 1057–1084.

Moecher, D. P., Essene, E. J. & Anovitz, L. M. 1988. Calculation and application of clinopyroxene–garnet–plagioclase–quartz geobarometers. *Contrib. Mineral. Petrol.* **100**, 92–106.

Mohanty, S. & Ramsay, J. G. 1994. Strain partitioning in ductile shear zones: an example from a Lower Pennine nappe of Switzerland. *J. Struct. Geol.* **16**, 663–676.

Naruk, S. J. 1986. Strain and displacement across the Pinateno Mountain shear zone, Arizona, U.S.A. *J. Struct. Geol.* **8**, 35–46.

Newman, J. & Mitra, G. 1993. Lateral variations in mylonite zone thickness as influenced by fluid–rock interactions, Linville Falls fault, North Carolina. *J. Struct. Geol.* **15**, 849–863.

O'Hara, K. 1988. Fluid flow and volume loss during mylonitization—an origin for phyllonite in an overthrust setting, North Carolina, U.S.A. *Tectonophysics* **156**, 21–36.

O'Hara, K. 1990. State of strain in mylonites from the western Blue Ridge province, southern Appalachians: the role of volume loss. *J. Struct. Geol.* **12**, 419–430.

Osberg, P. H. 1971. An equilibrium model for Buchan-type metamorphic rocks, south-central Maine. *Am. Mineral.* **56**, 570–585.
Panozzo, R. 1987. Two-dimensional strain determination by the inverse SURFOR wheel. *J. Struct. Geol.* **7**, 115–119.
Platt, J. P. & Vissers, R. L. 1980. Extensional structures in anisotropic rocks. *J. Struct. Geol.* **2**, 397–410.
Powell, R. 1985. Regression diagnostics and robust regression in geothermometer/geobarometer calibration: the garnet–clinopyroxene geothermometer revisited. *J. Metam. Geol.* **3**, 231–243.
Ramberg, H. 1975. Particle paths, displacement and progressive strain applicable to rocks. *Tectonophysics* **28**, 1–37.
Ramsay, J. G. 1980. Shear zone geometry: a review. *J. Struct. Geol.* **2**, 83–99.
Ramsay, J. G. & Allison, I. 1979. Structural analysis of shear zones in an Alpinised Hercynian granite, Maggia Nappen, Pennine Zone, Central Alps. *Schweiz. Miner. Petrogr. Mitt.* **59**, 251–279.
Ramsay J. G. & Graham, R. H. 1970. Strain variation in shear belts. *Can. J. Earth Sci.* **7**, 786–813.
Ramsay, J. G. & Huber, M. I. 1983. *The Techniques of Modern Structural Geology, Vol. 1: Strain Analysis.* Academic Press, Inc. London.
Ramsay, J. G. & Huber, M. I. 1987. *The Techniques of Modern Structural Geology, Vol. 2: Folds and Fractures.* Academic Press, Inc. London.
Saxena, S. K. & Ribbe, P. H. 1972. Activity-composition relations in feldspars. *Contrib. Mineral. Petrol.* **37**, 131–138.
Schedl, A., McCabe, C., Montanez, I. P., Fullagar, P. D. & Valley, J. W. 1992. Alleghenian regional diagenesis—a response to the migration of modified metamorphic fluids derived from beneath the Blue Ridge—Piedmont thrust sheet. *J. Geol.* **100**, 339–352.
Schwerdtner, W. M. 1982. Calculation of volume change in ductile band structures. *J. Struct. Geol.* **4**, 57–62.
Simpson, C. 1983. Strain and shape fabric variations associated with ductile shear zones. *J. Struct. Geol.* **5**, 61–72.
Strand, T. & Kulling, O. 1972. *Scandinavian Caledonides.* Wiley, London.

APPENDIX

Geothermometry and geobarometry

Mineral compositions were determined by electron microprobe analysis in order to calculate the pressures and temperatures of equilibration. Textural evidence for equilibration of all phases was observed under the petrographic microscope (i.e. sharp, well-defined grain boundaries) except for plagioclase which is partially replaced by clinozoisite and trace amounts of hematite after iron silicates and oxides. These textures probably developed during mild retrogression or weathering.

Electron microprobe analysis was performed on a JEOL 733 electron microprobe at the U.S. Bureau of Mines laboratory in Minneapolis, Minnesota. The operating conditions were 15 keV and 10 nA. Counts were collected for 4 s or until the standard deviation of the counting rate fell below 1%. At least five analyses of each mineral from several selected clusters or mosaics (Osberg 1971) were performed for assemblages in the amphibolite wall rock and shear zone. Well characterized oxides and silicates were used as standards and elemental weight% data was determined from the K-ratios using the program CITZAF (Armstrong 1989). The results from representative mosaics are presented in Table 5.

The mineral compositions within mosaics and from different mosaics both in and outside the shear zone are homogeneous (Table 5) except for plagioclase which has partially reacted to clinozoisite. Plagioclase compositions are relatively sodic (An_{33}) and homogeneous in the wall rock, but are highly variable within the recrystallized plagioclase phenocrysts which are partially sausseritized. Spot analyses of plagioclase in the interior of the recrystallized clusters reveals highly calcic plagioclase compositions, up to An83. The average plagioclase composition within the shear zone is intermediate (An_{67}), but the compositions are moderately variable within this domain. The consistency of other mineral compositions and Mg–Fe partitioning between hornblende and garnet within the shear zone and wall rock indicates equilibration of the assemblages near the peak of metamorphism.

The garnet–clinopyroxene thermometer yields a temperature of 792°C for the wall rock assemblage of the amphibolite using the calibration of Powell (1985). The garnet activity model of Berman (1990) and a single site, ideal solid solution model for clinopyroxene were used to calculate this temperature at an assumed pressure of 5 kb. Similar temperatures were calculated for the wall rock (782°C) and shear zone (810°C) assemblages using the garnet–hornblende thermometer (Graham & Powell, 1984). No activity coefficient corrections were necessary for Mg–Fe mass action between garnet and hornblende because the thermometer was calibrated using uncorrected equilibrium constants.

Garnet + clinopyroxene + plagioclase + quartz geobarometry yields pressures of 11.5 and 14.5 kb and the Mg and Fe end member reactions, respectively, using the more sodic plagioclase compositions (An_{33}) in the matrix of the amphibolite sample. These pressures were determined from the calibration of Moecher *et al.* (1988). When the most calcic plagioclase composition is used, however, this barometer yields pressures of 10.0 and 11.5 kb. In both cases, the activity models of Berman (1990) for garnet quaternary solid solutions and Saxena & Ribbe (1972) for the anorthite activity in plagioclase were applied in these calculations. The latter pressures are very close to the 8.8 kb pressure calculated using the Mg-end member garnet + hornblende + plagioclase + quartz geobarometer using model 2 (verbatim) of Kohn & Spear (1989). Using the same barometer, the shear zone assemblage yields a pressure of 8.7 kb for a plagioclase composition of An_{83}, and a pressure of 9.3 kb using a plagioclase composition of An_{67}. Calculated pressures using the most sodic plagioclase (An_{33}), Fe-end member reaction, and both end member model 1 calibrations, however, are considerably lower than those given above, but are less reliable because of the uncertain oxidation state of the iron.